Mon. Not. R. Astron. Soc. **389,** 1209–1217 (2008) doi:10.1111/j.1365-2966.2008.13442.x

The structures of embedded clusters in the Perseus, Serpens and Ophiuchus molecular clouds

S. Schmeja,[1,2]⋆ M. S. N. Kumar[1] and B. Ferreira[3]

[1]*Centro de Astrofísica da Universidade do Porto, Rua das Estrelas, 4150-762 Porto, Portugal*
[2]*Zentrum für Astronomie der Universität Heidelberg, Institut für Theoretische Astrophysik, Albert-Ueberle-Str 2, 69120 Heidelberg, Germany*
[3]*Department of Astronomy, University of Florida, Gainesville, FL 32611-2055, USA*

Accepted 2008 May 8. Received 2008 April 30; in original form 2008 February 29

ABSTRACT

The young stellar population data of the Perseus, Ophiuchus and Serpens molecular clouds are obtained from the *Spitzer* Cores to Discs (c2d) legacy survey in order to investigate the spatial structure of embedded clusters using the nearest-neighbour (NN) and minimum-spanning tree method. We identify the embedded clusters in these clouds as density enhancements and analyse the clustering parameter $\mathcal{Q}$ with respect to source luminosity and evolutionary stage. This analysis shows that the older Class 2/3 objects are more centrally condensed than the younger Class 0/1 protostars, indicating that clusters evolve from an initial hierarchical configuration to a centrally condensed one. Only IC 348 and the Serpens core, the older clusters in the sample, show signs of mass segregation (indicated by the dependence of $\mathcal{Q}$ on the source magnitude), pointing to a significant effect of dynamical interactions after a few Myr. The structure of a cluster may also be linked to the turbulent energy in the natal cloud as the most centrally condensed cluster is found in the cloud with the lowest Mach number and vice versa. In general, these results agree well with theoretical scenarios of star cluster formation by gravoturbulent fragmentation.

Key words: methods: statistical – stars: formation – ISM: clouds – ISM: kinematics and dynamics – open clusters and associations: general – infrared: stars.

1 INTRODUCTION

It is believed that stars form from high-density regions in turbulent molecular clouds that become gravitationally unstable, fragment and collapse. That way, a star cluster is built up in a complex interplay between gravity and supersonic turbulence (Mac Low & Klessen 2004; Ballesteros-Paredes et al. 2007; McKee & Ostriker 2007). Therefore, the structure of an embedded cluster, i.e. the spatial distribution of its members, may hold important clues about the formation mechanism and initial conditions. Several characteristics of star-forming clusters seem to be correlated with the turbulent flow velocity, for example, the star formation efficiency (Klessen, Heitsch & Mac Low 2000; Clark & Bonnell 2004; Schmeja, Klessen & Froebrich 2005), mass accretion rates (Schmeja & Klessen 2004) or the core mass distribution (Ballesteros-Paredes et al. 2006) and the initial mass function (Padoan & Nordlund 2005).

Giant molecular cloud (GMC) complexes usually contain multiple embedded clusters as well as more distributed, rather isolated young stellar objects (YSOs). The interstellar medium shows a hierarchical structure (sometimes described as fractal) from the largest GMC scales down to individual cores and clusters, which are sometimes hierarchical themselves. There is no obvious change in morphology at the cluster boundaries, so clusters can be seen as the bottom parts of the hierarchy, where stars have had the chance to mix (Efremov & Elmegreen 1998; Elmegreen et al. 2000; Elmegreen 2006).

Since embedded stars are best visible in the infrared part of the spectrum, and since nearby GMCs can span several degrees on the sky, wide-field near-infrared (NIR) and mid-infrared (MIR) surveys are useful tools for identifying and mapping the distribution of young stars in GMCs. The advent of the *Spitzer Space Telescope* has in particular led to large advances in such studies. The *Spitzer* Cores to Discs (c2d) legacy programme survey (Evans et al. 2003) aimed at mapping five large nearby star-forming regions, including Perseus, Serpens and Ophiuchus using *Spitzer's* IRAC (3.6 to 8 μm) and MIPS (24 to 160 μm) instruments (Harvey et al. 2006, 2007a,b; Jørgensen et al. 2006; Rebull et al. 2007; Padgett et al. 2008).

The Perseus molecular cloud complex is an extended region of low-mass star formation containing the well-studied embedded clusters IC 348 and NGC 1333. The latter is considered to be significantly younger (<1 Myr; Lada, Alves & Lada 1996; Wilking et al. 2004) than IC 348 (∼3 Myr; Luhman et al. 2003; Muench et al. 2007). The distance to the Perseus cloud is uncertain and

⋆E-mail: sschmeja@ita.uni-heidelberg.de

may lie somewhere between 200 and 320 pc, presumably there is a distance gradient along the cloud (see e.g. the discussion in Enoch et al. 2006). Areas of 3.86 deg^2 and 10.6 deg^2 have been mapped by IRAC and MIPS, respectively (Jørgensen et al. 2006; Rebull et al. 2007). Jørgensen et al. (2006) identified a total number of 400 YSOs, thereof 158 in IC 348 and 98 in NGC 1333, which means that a significant fraction of young stars is found outside the main clusters (see also Hatchell et al. 2005). Muench et al. (2007), also based on *Spitzer* MIR data, report a known membership of IC 348 of 363 sources and estimate a total population of more than 400.

The Serpens molecular cloud is a very active star-forming region covering more than 10 deg^2 on the sky at a distance of about 260 pc (Straižys, Černis & Bartašiūtė 1996). Areas of 0.89 deg^2 and 1.5 deg^2 have been mapped by IRAC and MIPS, respectively (Harvey et al. 2006, 2007a). In this region, 235 YSOs have been identified by Harvey et al. (2007b). The age of the main cluster, called the Serpens cloud core, is estimated to be $\sim$2 Myr (Kaas et al. 2004).

The Ophiuchus (or ρ Ophiuchi) molecular cloud is one of the closest star-forming regions at a distance of about 135 pc (Mamajek 2008). Its main cluster, L1688, is the richest known nearby embedded cluster. It is very young, with an age of probably $<$1 Myr (Greene & Meyer 1995; Luhman & Rieke 1999). 14.4 deg^2 have been observed with MIPS, leading to the identification of 323 YSO candidates (Padgett et al. 2008).

In this paper, we analyse the structure and distribution of the young stellar population unveiled by the c2d programme in these nearby molecular clouds and compare the results to current theoretical scenarios of star formation. For this purpose, we retrieved the c2d point source catalogues of the Perseus, Serpens and Ophiuchus molecular clouds and applied two complementary statistical methods to identify embedded clusters and analyse their structures. The selection of the data set is described in Section 2; the statistical methods and their application to the data are explained in Section 3 and the results and discussion are presented in Sections 4 and 5.

2 DATA SELECTION

The third delivery of data from the c2d legacy project (Evans et al. 2005), which combines observations from the IRAC and MIPS cameras, was obtained from the c2d website.[1] The combined photometric catalogues for the Perseus, Ophiuchus and Serpens molecular clouds were retrieved. These catalogues are products resulting from extensive analysis of the photometric observations in the four IRAC bands (central wavelengths 3.6, 4.5, 5.8 and 8.0 μm) and the three MIPS bands covering the 24 to 160 μm wavelength range. The sensitivity of the survey is expected to sample objects down to 0.1–0.5 $M_\odot$ in all three clouds.

The delivery catalogues provide source identifications and classifications based on a consistent method of analysis for all the targets covered by the legacy survey as described by Evans et al. (2005). The catalogues contain positions, photometry and associated quality flags, source type such as point/extended source and source classification such as stars/galaxy/YSO. These catalogues focus on identifying and classifying YSOs and distinguishing them from stars and galaxies. Extensive analysis of the point sources using colour–colour and colour–magnitude diagrams, spectral indices in the observed bands, comparison with SWIRE (*Spitzer* Wide-area Infrared Extragalactic survey) data to remove galaxy and polycyclic aromatic hydrocarbon (PAH) emission contaminants is used for this purpose.

[1] http://ssc.spitzer.caltech.edu/legacy/c2dhistory.html

Table 1. Classification scheme.

Object type (Evans et al. 2005)	Classification, main criteria
Red	*Class 0/1*
Red1	(objects only visible at
Red2	wavelengths $\geq$ 8 μm)
YSOc_MP1_red	
YSOc_IR4+MP1_red	
YSOc_IR4	*Class 2/3*
YSOc_MP1	(objects visible at
YSOc_IR4+MP1	wavelengths $<$8 μm,
YSOc_IR4_PAH-em	SEDs with slopes
YSOc_IR4_star+dust(BAND)	typical for Class 2/3)
YSOc_IR4_red	
YSOc_MP1_PAH-em	
YSOc_MP1_star+dust(BAND)	
YSOc_IR4+MP1_PAH-em	
YSOc_IR4+MP1_star+dust(BAND)	
Star	*Stars*
Star+dust (BAND)	(SEDs fitted with photospheres)

In the present work, we use these catalogues to retrieve the stellar and YSO population in the three molecular clouds based on the source classification flags. Although YSOs are classified based on their spectral energy distributions (SEDs) and MIR colours, a certain degree of confusion is always present when the complete SEDs are not available and only a part of the SED is sampled. The IRAC and MIPS observations cover the wavelength range where the YSOs lend themselves for an effective classification; however, confusion arising due to partial sampling of the SED cannot be removed. Further, an edge-on Class 2 source can imitate a Class 1 source etc. when classification is made using partial SEDs. Based on the nature of the point source SED, which is represented by 19 different flags in the c2d catalogues, we group the point sources into three categories, namely stars (foreground/background and cloud members), YSOs in Class 0/1 phase and YSOs in Class 2/3 phase. While the c2d catalogue provides a distinct classification for stars, the YSOs are represented by 15 different object types. We use the thumb rule of grouping sources that are visible only in wavelengths longer than 8 μm into the Class 0/1 group and the remaining into the Class 2/3 group. This leads to the classification given in Table 1, where we relate the object types from Evans et al. (2005) and their characteristics to the common evolutionary classes. Our classification does not necessarily represent the 'true' nature of the objects, which would in some cases require data from wavelengths longer than provided by *Spitzer* and a more sophisticated SED modelling.

3 STATISTICAL METHODS

3.1 Nearest-neighbour method

While clusters are readily identifiable as peaks in stellar density maps, the exact delimitation of a cluster is difficult and will always be somewhat arbitrary, since all the embedded clusters are surrounded by an extended population of YSOs distributed throughout the clouds. Several methods to detect clusters in a field have been developed. Usually, they are based on stellar densities (derived, for example, from star counts or Nyquist binning) and consider

as clusters all regions above a certain deviation ($\sim$2–4σ) from the background level (e.g. Lada et al. 1991; Lada & Lada 1995; Kumar, Keto & Clerkin 2006; Froebrich, Scholz & Raftery 2007).

The nearest-neighbour (NN) method (von Hoerner 1963; Casertano & Hut 1985) estimates the local source density ρ_j by measuring the distance from each object to its jth NN, where the value of j is chosen depending on the sample size. There is a connection between the chosen j value and the sensitivity to those density fluctuations being mapped. A small j value increases the locality of the density measurements at the same time as increasing sensitivity to random density fluctuations, whereas a large j value will reduce that sensitivity at the cost of losing some locality. Through the use of Monte Carlo simulations, Ferreira & Lada (in preparation) find that a value of $j = 20$ is adequate to detect clusters with 10 to 1500 members.

The positions of the cluster centres are defined as the density-weighted enhancement centres (Casertano & Hut 1985)

$$x_{d,j} = \frac{\sum_i x_i \rho_j^i}{\sum_i \rho_j^i},$$

where x_i is the position vector of the ith cluster member and ρ_j^i the jth NN density around this object. These centres do not necessarily correspond to the density peaks.

3.2 Minimum-spanning tree and $\mathcal{Q}$

The second method makes use of a minimum-spanning tree (MST), a construct from graph theory, which is defined as the unique set of straight lines ('edges') connecting a given set of points without closed loops, such that the sum of the edge lengths is minimum (Kruskal 1956; Prim 1957). From the MST, we derive the mean edge length $\ell_{\rm MST}$. Cartwright & Whitworth (2004) introduced the parameter $\mathcal{Q} = \bar{\ell}_{\rm MST}/\bar{s}$, which combines the normalized correlation length $\bar{s}$, i.e. the mean distance between all stars, and the normalized mean edge length $\bar{\ell}_{\rm MST}$. The $\mathcal{Q}$ parameter permits to quantify the structure of a cluster and to distinguish between clusters with a central density concentration and hierarchical clusters with possible fractal substructure. Large $\mathcal{Q}$ values ($\mathcal{Q} > 0.8$) describe centrally condensed clusters having a volume density $n(r) \propto r^{-\alpha}$, while small $\mathcal{Q}$ values ($\mathcal{Q} < 0.8$) indicate clusters with fractal substructure. $\mathcal{Q}$ is correlated with the radial density exponent α for $\mathcal{Q} > 0.8$ and anti-correlated with the fractal dimension D for $\mathcal{Q} < 0.8$. The dimensionless measure $\mathcal{Q}$ is independent of the number of objects and of the cluster area. The method has been successfully applied to both observed clusters and results of numerical simulations (Cartwright & Whitworth 2004; Schmeja & Klessen 2006; Kumar & Schmeja 2007). For details of the method, in particular its implementation and normalization used for this study, see Schmeja & Klessen (2006).

3.3 Application to the data

The NN and MST statistical methods described above were applied to the c2d data of the Perseus, Serpens and Ophiuchus molecular clouds. We first used the NN analysis (described in detail by Ferreira et al., in preparation) on the stellar and YSO populations in the entire clouds to detect density enhancements and therefore embedded clusters. For this purpose, 20th NN density maps were generated for the full extent of the available c2d data. The 20th NN density is thought to be the optimum density to identify primary clusters and not pick up very loose groups (Ferreira & Lada, in preparation). We found that using only the point sources that were classified as YSOs to produce the NN maps yields the best density contrast and boundary identifications. We determined the average 20th NN density in the clouds away from the clusters and define as cluster members all YSOs whose density exceeds 3σ of the average value. The cluster boundaries are shown as thick lines in Fig. 1 and the density thresholds $\rho_{\rm thresh}$ for the clusters are given in Table 2.

All YSOs enclosed within the respective cluster defining contour are treated as cluster members. For those we constructed the MST and determined $\mathcal{Q}$.

Note that the exact definition of the cluster boundaries is only relevant for the quantitative structure analysis using the $\mathcal{Q}$ parameter. Changing the cluster definition criteria may change the absolute $\mathcal{Q}$ values, but it does not affect the general trends and correlations discussed below.

4 STRUCTURE ANALYSIS

4.1 Cluster morphology

The YSOs in the three investigated molecular clouds are found in the embedded clusters and in a distributed population that extends through the entire cloud (Jørgensen et al. 2006; Harvey et al. 2007b). Fig. 1 shows IRAC Channel 4 (8 μm) images of the four largest embedded clusters IC 348, NGC 1333, Serpens cloud core and L1688, overlaid with the 20th NN density contours.

In the Perseus molecular cloud, apart from the embedded clusters NGC 1333 and IC 348, the region around Barnard 3 (B3) emerges as a moderately sized cluster, but no significant density enhancements are found associated with L1455 and L1448. Despite the large number of member stars, the Perseus clusters show relatively small peak densities compared to the other clouds. Likewise, the Perseus cloud shows the lowest 'background' YSO density of all regions. The density peak in IC 348 coincides with the B5 star HD 281159, the most massive star in this cluster, whereas the two B stars in NGC 1333 (BD +30 549 and SVS 3) are not associated with the densest region. The B0 star HD 278942 is found close to the centre of the B3 cluster; however, it may be located behind the main Perseus cloud complex (Ridge et al. 2006).

In the Serpens cloud, two major clusters were detected: the main cluster in this cloud, usually called the Serpens cloud core, and referred to as Cluster A by Harvey et al. (2006), and a recently discovered cluster called Cluster B by Harvey et al. (2006) and Serpens/G3-G6 by Djupvik et al. (2006). The Serpens core has a very steep density gradient and a prominent peak with a density of 1045 pc^{-2}, the highest of all investigated clusters and twice the value of the second densest cluster.

In the Ophiuchus cloud, one highly structured, major embedded cluster was detected roughly centred on L1688, several smaller density enhancements clearly trace four filamentary structures that seem to converge on this prominent cluster. These density enhancements are in good correlation with the dust continuum emission maps. Two of these density enhancements are picked up as small clusters by the NN method, we designate them Ophiuchus north and centre. The Ophiuchus north cluster is centred around a group of bright B stars (ρ Oph D, ρ Oph AB, ρ Oph C).[2] Furthermore, we detect the known cluster associated with L1689S (Bontemps et al. 2001), which shows a single peak and no distinct substructure.

The shapes of IC 348, NGC 1333, Serpens A and L1689S can be roughly approximated by ellipses, whereas the hierarchical L1688

[2] These designations are not to be confused with the ones used for the subclusters discussed below and marked in Fig. 1.

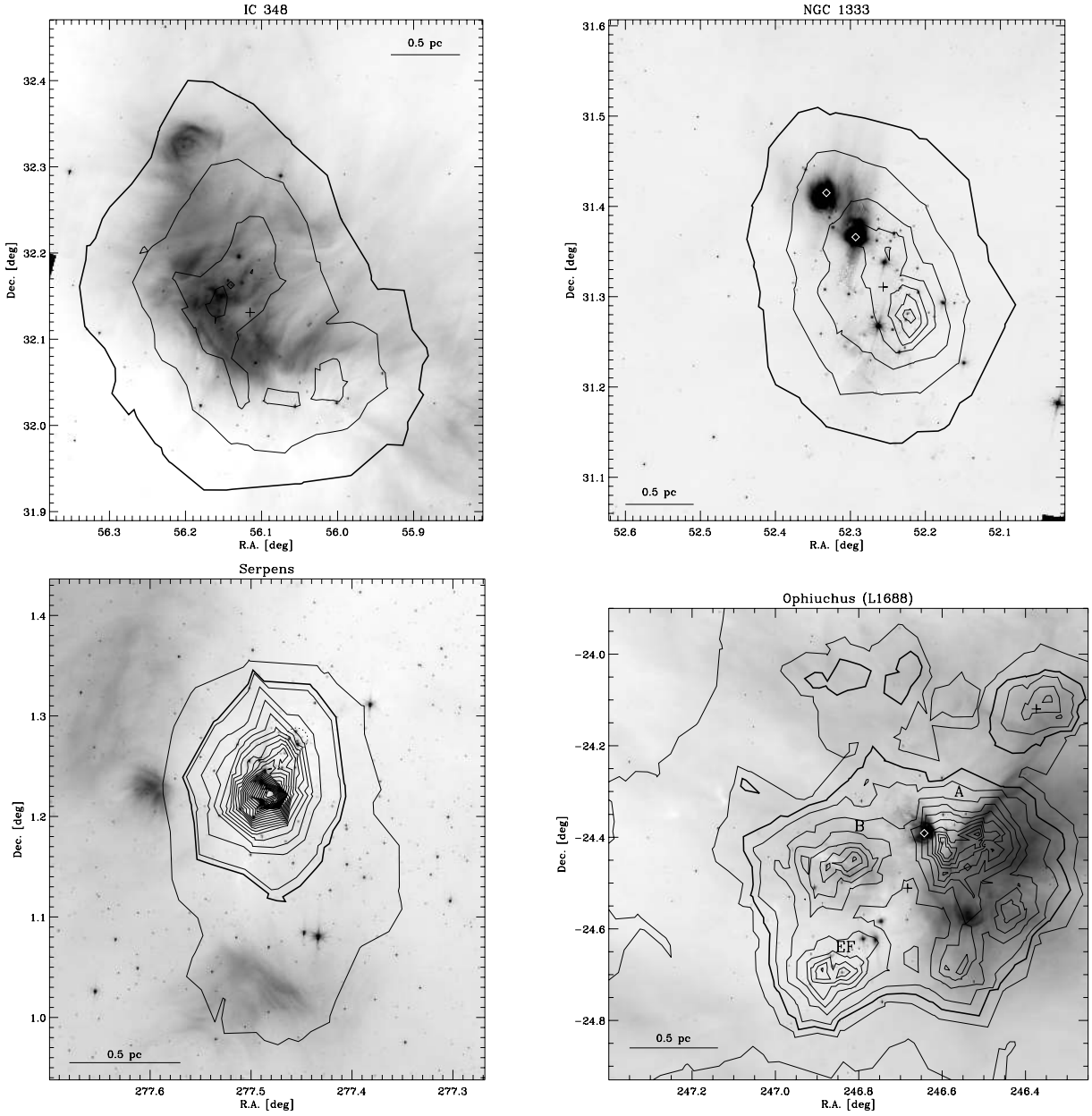

Figure 1. *Spitzer* IRAC Channel 4 (8 μm) images of the four main clusters IC 348, NGC 1333, Serpens A and L1688 overlaid with the 20th NN density contours. The thin contours are plotted in intervals of 40 pc^{-2}. The outermost thin contours correspond to a NN density of 40 pc^{-2}. The thick contours indicate the cluster boundaries as defined in the text. The horizontal bars showing a projected length of 0.5 pc are based on assumed distances of 315, 260 and 135 pc to the Perseus, Serpens and Ophiuchus cloud, respectively. Crosses indicate the cluster centres and the known B stars are highlighted by diamond symbols.

cluster shows an irregular, nevertheless rather circular, perimeter. It is interesting to note that the elliptical clusters appear to have two peaks roughly coinciding with the foci of ellipses. However, these peaks seem to consist of YSO populations of different evolutionary stages. This is seen in NGC 1333, with the density peak in the south and two luminous, massive B stars, which illuminate the prominent reflection nebula, in the north. In Serpens, we note a group of bright stars north of the density peak, marked by a dotted circle in Fig. 1. The second peak in IC 348, seen to the south-east, seems to correspond to a new star formation episode close to HH211 (Tafalla, Kumar & Bachiller 2006).

Table 2 lists all the detected embedded clusters along with their position, size, peak density, the $\mathcal{Q}$ parameter and the number of YSOs n_*. The size corresponds to the length of the major axis of an ellipse fitted to the cluster areas. Its only purpose is to provide the reader with a rough estimate of the diameter of the cluster. The linear sizes are computed assuming distances of 315, 260 and 135 pc to the Perseus, Serpens and Ophiuchus cloud, respectively.

4.2 $\mathcal{Q}$ values

Extensive analysis of the distribution of the MST edge lengths as a function of YSO class and the $\mathcal{Q}$ parameter as a function of YSO brightness was carried out only for four embedded clusters where the number statistics are significant and suitable for this kind of analysis. These four major embedded clusters are NGC 1333, IC 348, Serpens

Table 2. Clustering parameters of the identified clusters in the three regions.

Region/ cluster	RA (J2000) (deg)	Dec. (J2000) (deg)	Size (pc)	$\rho_{\rm thresh}$ (pc^{-2})	$\rho_{\rm peak}$ (pc^{-2})	n_*	$\mathcal{Q}$
Perseus							
NGC 1333	52.2563	+31.3107	2.09	20	261	158	0.81
IC 348	56.1151	+32.1310	2.53	20	140	204	0.80
Barnard 3	54.9612	+31.9227	1.67	20	45	51	0.69
Serpens							
Serpens core (A)	277.485	+1.2274	1.00	70	1045	84	0.84
Serpens B	277.256	+0.5059	0.77	70	378	43	0.77
Ophiuchus							
Ophiuchus north	246.348	−23.4660	0.78	95	126	34	0.68
Ophiuchus centre	246.374	−24.1197	0.52	95	213	29	0.73
L1688	246.683	−24.5112	1.85	95	509	337	0.72
L1689S	248.045	−24.9294	1.41	50	240	78	0.78

Table 3. Numbers of objects and $\mathcal{Q}$ values for the different evolutionary classes.

Cluster	Class 0/1		Class 2/3	
	n_* (per cent)	$\mathcal{Q}$	n_* (per cent)	$\mathcal{Q}$
NGC 1333	62 (39)	0.78	96 (61)	0.83
IC 348	72 (35)	0.71	132 (65)	0.78
Serpens A	33 (39)	0.85	51 (61)	0.85
L1688	194 (58)	0.69	143 (42)	0.78

Table 4. Clustering parameters of the subclusters in L1688.

Subcluster	RA (deg)	Dec. (deg)	$\rho_{\rm peak}$ (pc^{-2})	n_*	$\mathcal{Q}$
Oph A	246.553	−24.416	509	67	0.74
Oph B	246.836	−24.465	373	52	0.79
Oph EF	246.854	−24.679	367	43	0.77

core and L1688. It can be seen from Fig. 1 that the Serpens core, NGC 1333 and IC 348 clusters are centrally concentrated, although at very different surface densities, whereas L1688 shows at least four peaks enclosed within the cluster defining contour. This is reflected in the $\mathcal{Q}$ values listed in Table 2. L1688 shows the lowest $\mathcal{Q}$ value (0.72) indicating fractal substructure, whereas the other clusters show $\mathcal{Q}$ values of $\mathcal{Q} \geq 0.8$, denoting central condensation. All the small clusters have values of $\mathcal{Q} < 0.8$.

In Table 3, we list the absolute and relative numbers of Class 0/1 and Class 2/3 objects and their $\mathcal{Q}$ values in the four large embedded clusters. Note that the classifications (see Section 2) do not necessarily correspond to the standard definitions. Assuming that the ratio of younger to older sources represents the relative ages of the embedded clusters, the data in Table 3 indicate that the L1688 cluster is the youngest of all, NGC 1333 and Serpens are slightly older and IC 348 is the oldest of all four. This is not identical, but quite similar to the age estimates based on more sophisticated methods mentioned in Section 1. In all the clusters but Serpens, the $\mathcal{Q}$ values are significantly higher for the Class 2/3 objects than for the Class 0/1 protostars, indicating a more centrally condensed configuration for the older sources. In the centrally condensed Serpens A cluster, the two groups show the same $\mathcal{Q}$ values.

The three major subclusters in L1688 were investigated further, these are (following the nomenclature of Bontemps et al. 2001) Oph A, Oph B and Oph EF (marked in Fig. 1). They are defined as having NN densities $>180\,{\rm pc}^{-2}$ and their clustering properties are listed in Table 4. Oph A contains 41 Class 0/1 protostars and 26 Class 2/3 objects and has a value of $\mathcal{Q} = 0.74$ in the hierarchical range. Oph B (18 Class 0/1, 34 Class 2/3 sources) and Oph EF (16 Class 0/1, 27 Class 2/3 sources) show higher values of $\mathcal{Q} = 0.79$ and 0.77, respectively. Oph A is associated with a larger amount of gas and has a significantly higher Class 0/1 to Class 2/3 ratio than the other two subclusters, making it most likely the youngest of the subclusters; it also shows the lowest $\mathcal{Q}$ value of the subclusters. Again, we see an evolutionary sequence from the youngest, hierarchical cluster to the more evolved clusters closer to central condensation. When looking at Class 0/1 and Class 2/3 sources separately, we again find significantly higher $\mathcal{Q}$ values for the more evolved objects: in Oph A, the value rises from $\mathcal{Q} = 0.74$ for Class 0/1 to $\mathcal{Q} = 0.90$ for Class 2/3, in Oph B from 0.77 to 0.81 and in Oph EF from 0.73 to 0.79.

4.3 Distribution of MST edge lengths

The lengths of the MST edges can be seen as the separation from one object to its NN. Histograms of the MST edge lengths indicate characteristic separations for YSOs in each of the clusters. Fig. 2 shows the normalized histograms of the MST edge lengths in the four main clusters in bins of 0.02 pc, using the assumed distances given above (Section 4.1). The histograms show a distinct peak at 0.02 pc (Serpens, L1688) and 0.04 pc (NGC 1333), respectively, and the distributions spread up to separations of 0.2 to 0.3 pc. In IC 348, however, two peaks appear at a larger separation of 0.04 and 0.08 pc. Also shown in Fig. 2 are the same histograms for Class 0/1 and Class 2/3 sources separately. In the clusters NGC 1333, Serpens and L1688, we do not see a significant difference between the separations of Class 0/1 and Class 2/3 objects. Objects of all evolutionary states are more or less similarly distributed in the cluster. In IC 348, however, it is only the Class 2/3 objects that roughly follow the distribution of the overall cluster members, whereas the Class 0/1 objects seem to be homogeneously distributed. This is because the central cluster in IC 348 is evolved and has blown out a cavity, with the current star formation occurring in a shell around the cluster (Tafalla et al. 2006; Muench et al. 2007).

The characteristic edge lengths found from Fig. 2 do reflect the true separations and are not a result of poor spatial sampling

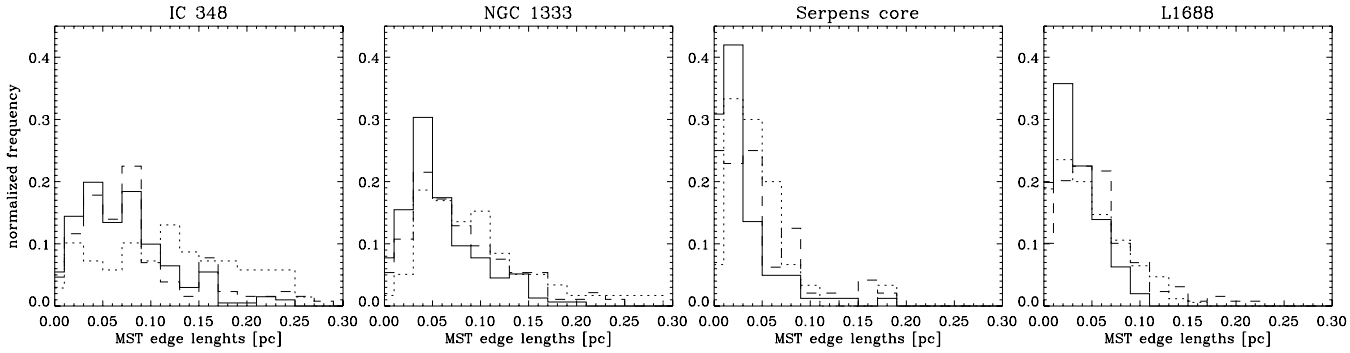

Figure 2. Normalized histograms of MST edge lengths for Class 0/1 (dotted line), Class 2/3 (dashed line) and all YSOs (solid line) in the four main clusters.

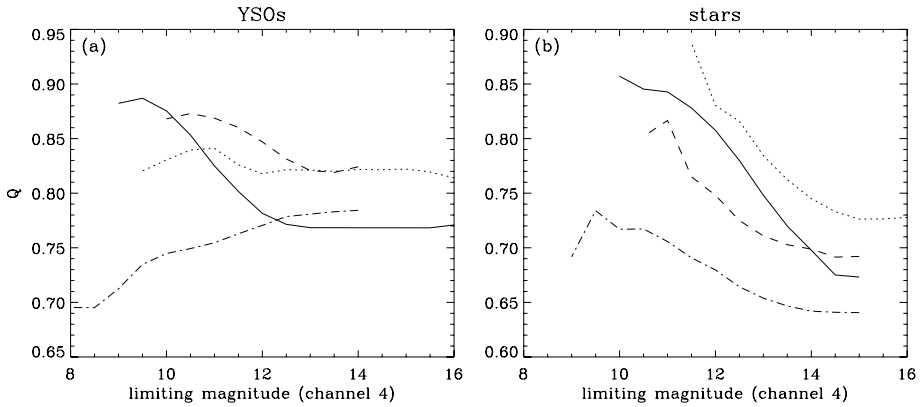

Figure 3. $\mathcal{Q}$ as a function of source magnitude for YSOs (left-hand panel) and stars (right-hand panel) in Channel 4 for IC 348 (solid line), NGC 1333 (dotted line), Serpens A (dashed line) and L1688 (dash–dotted line).

because these values are almost an order of magnitude higher than the tolerance used for matching IRAC and MIPS data (4 arcsec, corresponding to 0.003–0.006 pc). We also investigated the MSTs and their edge lengths for the stars in the cluster field, but due to their large spatial density they would generally yield very short edges and a narrow peak of the distribution at very small projected separations.

4.4 $\mathcal{Q}$ versus magnitude

Assuming that the IR source magnitudes are representative of the source masses and evolutionary stages, we investigate the variation of $\mathcal{Q}$ as a function of magnitude. $\mathcal{Q}$ was calculated for sources brighter than a certain magnitude in steps of 0.5 mag as long as the sample contained at least 40 objects. This calculation was made for YSOs and stars separately. The resulting $\mathcal{Q}$ versus Channel 4 magnitude curves for YSOs and stars are shown in Figs 3(a) and (b), respectively. (Similar plots were made using Channel 1, 2 and 3 magnitude as well; they look similar in all bands.) The results for different clusters are shown using different line styles. Fig. 3(a) shows that the YSO curves remain flat or rising with magnitude for the clusters NGC 1333 and L1688 while they decrease with magnitude for IC 348 and, less pronounced, for Serpens. This implies that in NGC 1333 and L1688, YSOs of all luminosities display a roughly similar configuration, whereas in Serpens and IC 348 the low-luminosity YSOs are less centrally concentrated than the more luminous YSOs.

In contrast, the stellar population shows a declining $\mathcal{Q}$ versus magnitude curve for all the clusters, indicating that the fainter stars are relatively homogeneously distributed in space and the brighter stars are centrally concentrated. Since this curve is computed for a region encompassing only the dense cluster, the chances of picking up fainter background sources through the large column of extinction are low. Due to the same reason, stars that are cluster members outnumber foreground stars for the computed area. Therefore, the observed effect is representative of the true variations among the cluster members. Furthermore, a random distribution expected from foreground or background objects will produce a $\mathcal{Q}$ value constant over the whole magnitude range at $\mathcal{Q} \approx 0.73$ and cannot reproduce the declining curve seen in Fig. 3(b).

Assuming the age of IC 348 as 3 Myr, that of Serpens as 2 Myr and that of NGC 1333 and L1688 around 1 Myr (see Section 1), the YSO curves in Fig. 3(a) show that the brighter objects appear to evolve towards centrally condensed configurations and fainter objects towards homogeneous distributions with time. The transition of the distribution of the lowest-mass/substellar objects from a centrally condensed configuration to a more homogeneous distribution is thought to be an effect of dynamical evolution. A detailed discussion of this effect in IC 348 and the Orion Trapezium cluster and its implications for the formation of brown dwarfs can be found in Kumar & Schmeja (2007).

5 DISCUSSION

5.1 Dynamical evolution and mass segregation

The structure analysis of YSOs and stars presented in the previous section has several implications. The significantly higher $\mathcal{Q}$ values

for the Class 2/3 objects compared to the Class 0/1 protostars show that the older sources are more centrally condensed than the younger objects, which in most cases show a hierarchical configuration. Also in other embedded clusters, the Class 0/1 protostars are found in subclusters, e.g. in NGC 2264 (Teixeira et al. 2006) or the Orion Trapezium cluster (Lada et al. 2004). This is in agreement with the predictions of numerical simulations (Bonnell, Bate & Vine 2003; Schmeja & Klessen 2006) suggesting that clusters build up from several subclusters that eventually form a single centrally condensed cluster. However, it is not possible to distinguish between the structure inherent to the cloud and that arising due to dynamical evolution. It is tempting to assume that the Class 0/1 objects trace the structure inherent to the cloud while the older objects represent the structure as a result from dynamical evolution. More than half of the mass of a Class 0 protostar is found in its envelope. So, a Class 0 source can be seen as still part of the cloud, while the older YSOs are star-like objects with a disc rather than an envelope and are therefore susceptive to dynamical interaction.

While $\mathcal{Q}$ rises as a cluster evolves, its absolute value does not depend on the age of the cluster. NGC 1333 and IC 348 with estimated ages of 1 and 3 Myr, respectively, have similar $\mathcal{Q}$ values of 0.81 and 0.80, whereas the two extreme $\mathcal{Q}$ values in our sample (0.84 and 0.72) are associated with the clusters L1688 and Serpens thought to have ages of about 1 and 2 Myr, respectively. This shows that the cluster structure in general is not directly correlated with the evolutionary stage and rather depends on the existing large-scale structure of the cloud, but the observation that Class 2/3 objects (which had more time and are also more susceptive to dynamical interactions) are more centrally condensed than the younger protostars is a clue that the cluster evolves from a hierarchical to a more centrally condensed configuration as predicted by numerical simulations.

We interpret the decrease of $\mathcal{Q}$ with fainter (i.e. less massive) sources as an effect of mass segregation. However, the relation of luminosity to mass may be different for the different evolutionary classes, which may cause some interference of evolutionary and mass segregation effects. The trend shown in Fig. 3(a), based on Channel 4 (8 μm) magnitudes, is mainly representative of Class 2/3 objects, but it is similar in the other IRAC bands, and also in MIPS Channel 1 (24 μm), which includes Class 0/1 objects.

A decrease of $\mathcal{Q}$ with fainter magnitudes is seen in IC 348 (∼3 Myr) and, to a somewhat lesser extent, in Serpens (∼2 Myr), whereas there are no signs of mass segregation in the YSO population of the youngest clusters. The stellar (i.e. older) population, on the other hand, shows significant mass segregation in all clusters. Therefore, mass segregation seems to be a function of age. According to simulations of turbulent molecular clouds (Bonnell et al. 2003), YSOs form at different locations in the cloud and condense into a single cluster within a few free-fall times or less than 1 Myr. Dynamical interactions become important only after this initial assembly of YSOs is made. In particular, dynamical mass segregation occurs on a time-scale of the order of the relaxation time of the cluster (Bonnell & Davies 1998). This is consistent with the observed effects. Our findings are not necessarily contradicting claims that mass segregation is primordial, i.e. massive stars form near or in the centre of a cluster (Bonnell & Davies 1998). In the youngest clusters, contrary to the older ones, the massive YSOs show a more hierarchical distribution (smaller $\mathcal{Q}$; see Fig. 3a) than the lower-mass objects, suggesting that the massive stars are still on the bottom of the potential wells of the former subclusters. This is consistent with theoretical scenarios in which mergers of small clumps that are initially mass segregated (or in which mass segregation is generated quickly by two-body relaxation) lead to larger clusters that are also mass segregated (McMillan, Vesperini & Portegies Zwart 2007).

Table 5. Gas properties and Mach numbers.

Cluster	Δv (km s^{-1})	T (K)	c_s (km s^{-1})	$\mathcal{M}$	$\mathcal{Q}$	Ref.[a]
Serpens A	0.77	12	0.21	3.8	0.84	1
NGC 1333	0.95	13	0.21	4.5	0.81	1
L1688	1.33	15	0.23	5.8	0.72	2

[a]References for Δv and T: (1) Jijina et al. (1999) and (2) Myers et al. (1978).

The NN maps (Fig. 1) indicate that IC 348, NGC 1333 and Serpens A have formed from a single dense core, while L1688 appears to lie at the interface of merging filaments (Ferreira et al., in preparation). L1688 has a highly hierarchical structure and consists of at least three readily identifiable subclusters; nevertheless, it is detected as a single cluster by the 20th NN maps, whose centre does not coincide with any of the subclusters. Provided this geometrical centre corresponds approximately to the centre of mass and provided the density is high enough, the subclusters may merge to form a single centrally condensed cluster in the future. The structure of the cluster seems to be correlated to the cloud structure in the sense that the collapse of a single dense core more easily leads to a centrally condensed cluster, while interacting filaments are reflected in a longer-lasting hierarchical structure of the cluster.

5.2 Turbulence and cluster structure

As turbulence seems to play an important role in the build-up of a star cluster (Elmegreen et al. 2000; Mac Low & Klessen 2004; Ballesteros-Paredes et al. 2007), we investigate the relation of the cluster structure with the turbulent environment. In Table 5, we list the velocity dispersion Δv and temperature T of the dense gas and the derived Mach numbers in Serpens, NGC 1333 and L1688 as traced by NH_3 line observations (Myers et al. 1978; Jijina, Myers & Adams 1999). The NH_3 line is a tracer of dense gas which is representative of the cores from which star clusters are born (Bergin & Tafalla 2007) and is also the tracer that is least affected by outflows. Therefore, the NH_3 linewidths better represent the turbulent properties of the cluster forming cores than other tracers of the molecular cloud such as CO or CS, which may be seriously affected by the presence of outflows and effects of molecular depletion (Tafalla et al. 2002; Bergin & Tafalla 2007). Similarly, the best measure of the core temperatures is also obtained from the same emission lines. Hence, we use the observed values of Δv and T from this tracer to compute the Mach number $\mathcal{M} = \Delta v/c_s$ where the isothermal sound speed $c_s = (RT/\mu)^{1/2}$ with the specific gas constant R and the mean molecular weight $\mu = 2.33$. Myers, Ladd & Fuller (1991) argue that core linewidths are dominated by non-thermal motions (turbulence) only for core masses above ∼22 $M_\odot$ and that linewidths are thermal below ∼7 $M_\odot$. Since the core masses in all three clouds are above ∼30 $M_\odot$ at an $A_V \approx 20$ mag contour (Enoch et al. 2007), the assumption that the linewidths are caused by turbulence is justified. The findings of Myers et al. (1991) also lead to the conclusion that cluster-forming cores are turbulent while quiescent cores form isolated stars (see also Myers 2001).

Comparing the Mach numbers and $\mathcal{Q}$ values in Table 5 shows that Serpens, being the most centrally condensed cluster, is associated with the lowest Mach number (turbulent energy) and L1688

being the most hierarchically structured cluster is associated with the highest Mach number. Note that we compare $\mathcal{Q}$ and $\mathcal{M}$ only for the three clusters that have a significant population of YSOs, are embedded in dense gas and have similar ages of 1–2 Myr. For this reason, we excluded IC 348 from this comparison, which is significantly older and largely depleted of cold gas. Since $\mathcal{Q}$ seems to depend on the temporal evolution, a comparison only makes sense for clusters of roughly the same age.

These results are in accordance with the scenario of turbulent fragmentation and hierarchical formation of clusters. Numerical simulations demonstrate that high Mach number flows lead to a highly fragmented density structure (Ballesteros-Paredes et al. 2006). Enoch et al. (2007) study the same clusters and obtain a contradictory result; however, the Mach numbers they compute are based on velocity dispersions obtained from observations of the CO molecule, which rather traces the outer envelope of the molecular cloud and may be contaminated by the effects of outflows.

As this correlation is obviously based on small-number statistics and has not been found in numerical simulations of gravoturbulent fragmentation (Schmeja & Klessen 2006) and considering the associated uncertainties of Δv and T, it has to remain rather speculative. Nevertheless, it is a hint that the structure of an embedded cluster may be somehow connected to the turbulent environment. Even though the turbulent velocity is probably not the only agent responsible for shaping the cluster, it may play a significant role. While a high degree of turbulence in the cloud may keep the young stars in a more hierarchical distribution for a longer time, the absence of strong turbulent motions may help to reach a centrally condensed configuration more quickly. Assuming that strong turbulence in the cloud also leads to a high-velocity dispersion among the embedded stars, this is also supported by the results of Goodwin & Whitworth (2004), who performed *N*-body simulations of the dynamics of fractal star clusters in order to investigate the evolution of substructure in recently formed clusters. They show that if the velocity dispersion in the cluster is low, much of the substructure will be erased; however if the velocity dispersion is high, significant levels of substructure can survive for several crossing times.

6 SUMMARY

We used the *Spitzer* c2d survey data of the nearby molecular clouds Perseus, Serpens and Ophiuchus to identify embedded clusters and analyse their structures using the NN and MST method. Apart from the large known embedded clusters IC 348, NGC 1333, Serpens core and L1688, we only found a few relatively small clusters. The $\mathcal{Q}$ parameter was determined for all embedded clusters in these clouds and the MST edge lengths and $\mathcal{Q}$ values were analysed as a function of YSO class and magnitudes. Our main results can be summarized as follows.

(i) Among the four large clusters, IC 348, NGC 1333 and Serpens are centrally condensed ($\mathcal{Q} \gtrsim 0.8$), while L1688 shows a hierarchical structure with several density peaks. The three main subclusters in L1688 show again a hierarchical structure, with Oph A, presumably the youngest one, having the lowest $\mathcal{Q}$ value. The peak densities vary strongly between the clusters in different clouds, as does the density of the dispersed YSO population.

(ii) In all clusters, the $\mathcal{Q}$ values for the younger Class 0/1 objects are substantially lower than for the more evolved Class 2/3 objects. This indicates that embedded clusters are assembled from an initial hierarchical configuration arising from the filamentary parental cloud and eventually end up as a single centrally condensed cluster, as predicted by numerical simulations of turbulent fragmentation. While the youngest, deeply embedded objects may represent the structure inherent to the cloud, the distribution of the older objects probably is a result from dynamical interactions.

(iii) We find no signs of mass segregation for the YSOs in the youngest clusters, but only for the YSO population in the presumably older clusters Serpens and IC 348. In contrast, the stellar population displays a clear mass segregation in all clusters. This suggests that the effect of dynamical interaction becomes visible at a cluster age between about 2 and 3 Myr.

(iv) The structure of a cluster may be related to the turbulent velocity in the cloud in a way that clusters in regions with low Mach numbers reach a centrally condensed configuration much faster than those in highly turbulent clouds, in agreement with *N*-body simulations (Goodwin & Whitworth 2004).

The results from the Perseus, Serpens and Ophiuchus star-forming regions are in good agreement with the predictions of theoretical scenarios claiming that embedded clusters form from gravoturbulent fragmentation of molecular clouds in a hierarchical process. Our results may not be applicable to the YSO populations in other regions, in particular the Taurus star-forming region, which shows a level of clustering and velocity dispersions very different from the regions studied in this work and which is generally harder to reconcile with the gravoturbulent scenario (Froebrich et al. 2006).

ACKNOWLEDGMENTS

This work is based on observations made with the *Spitzer Space Telescope*, which is operated by the Jet Propulsion Laboratory, California Institute of Technology under a contract with NASA. SS and MSNK were supported by a research grant POCTI/CFE-AST/55691/2004 approved by Fundação para a Ciência e a Tecnologia (FCT) and Programa Operacional 'Ciência, Tecnologia, Inovação', with funds from the European Regional Development Fund. SS also acknowledges funding by the Deutsche Forschungsgemeinschaft (grant SCHM 2490/1-1) during part of this work. MSNK is also supported by the project PTDC/CTE-AST/65971/2006 approved by FCT. BF wants to acknowledge support from his PhD advisor Elizabeth Lada as well as financial support from NSF grant AST 02-02976 and National Aeronautics and Space Administration grant NNG 05D66G issued to the University of Florida.

REFERENCES

Ballesteros-Paredes J., Gazol A., Kim J., Klessen R. S., Jappsen A.-K., Tejero E., 2006, ApJ, 637, 384
Ballesteros-Paredes J., Klessen R. S., Mac Low M.-M., Vázquez-Semadeni E., 2007, in Reipurth B., Jewitt D., Keil K., eds, Protostars and Planets V. Univ. of Arizona Press, Tucson, p. 63
Bergin E. A., Tafalla M., 2007, ARA&A, 45, 339
Bonnell I. A., Davies M. B., 1998, MNRAS, 295, 691
Bonnell I. A., Bate M. R., Vine S. G., 2003, MNRAS, 343, 413
Bontemps S. et al., 2001, A&A, 372, 173
Cartwright A., Whitworth A. P., 2004, MNRAS, 348, 589
Casertano S., Hut P., 1985, ApJ, 298, 80
Clark P. C., Bonnell I. A., 2004, MNRAS, 347, L36
Djupvik A. A., André P., Bontemps S., Motte F., Olofsson G., Gålfalk M., Florén H.-G., 2006, A&A, 458, 789
Efremov Y. N., Elmegreen B. G., 1998, MNRAS, 299, 588
Elmegreen B. G., 2006, in Richtler T., Larsen S., eds, Globular Clusters – Guides to Galaxies. ESO/Springer, Berlin, in press (astro-ph/0605519)

Elmegreen B. G., Efremov Y., Pudritz R. E., Zinnecker H., 2000, in Mannings V., Boss A. P., Russell S. S., eds, Protostars and Planets IV. Univ. of Arizona Press, Tucson, p. 179
Enoch M. L. et al., 2006, ApJ, 638, 293
Enoch M. L., Glenn J., Evans N. J., II, Sargent A. I., Young K. E., Huard T. L., 2007, ApJ, 666, 982
Evans N. J., II, et al., 2003, PASP, 115, 965
Evans N. J., II, et al., 2005, Third Delivery of Data from the c2d Legacy Project: IRAC and MIPS, Spitzer Science Center, Pasadena, http://data.spitzer.caltech.edu/popular/c2d/20051220 _enhanced_v1/Documents/C2D_Explan_Supp.pdf
Froebrich D., Schmeja S., Smith M. D., Klessen R. S., 2006, MNRAS, 368, 435
Froebrich D., Scholz A., Raftery C. L., 2007, MNRAS, 374, 399
Goodwin S. P., Whitworth A. P., 2004, A&A, 413, 929
Greene T. P., Meyer M. R., 1995, ApJ, 450, 233
Harvey P. M. et al., 2006, ApJ, 644, 307
Harvey P. M. et al., 2007a, ApJ, 663, 1139
Harvey P., Merín B., Huard T. L., Rebull L. M., Chapman N., Evans N. J., II, Myers P. C., 2007b, ApJ, 663, 1149
Hatchell J., Richer J. S., Fuller G. A., Qualtrough C. J., Ladd E. F., Chandler C. J., 2005, A&A, 440, 151
Jijina J., Myers P. C., Adams F. C., 1999, ApJS, 125, 161
Jørgensen J. K. et al., 2006, ApJ, 645, 1246
Kaas A. A. et al., 2004, A&A, 421, 623
Klessen R. S., Heitsch F., Mac Low M.-M., 2000, ApJ, 535, 887
Kruskal J. B. Jr, 1956, Proc. Am. Math. Soc., 7, 48
Kumar M. S. N., Schmeja S., 2007, A&A, 471, L33
Kumar M. S. N., Keto E., Clerkin E., 2006, A&A, 449, 1033
Lada E. A., Lada C. J., 1995, AJ, 109, 1682
Lada C. J., Alves J., Lada E. A., 1996, AJ, 111, 1964
Lada E. A., Evans N. J., II, Depoy D. L., Gatley I., 1991, ApJ, 371, 171
Lada C. J., Muench A. A., Lada E. A., Alves J. F., 2004, AJ, 128, 1254
Luhman K. L., Rieke G. H., 1999, ApJ, 525, 440
Luhman K. L., Stauffer J. R., Muench A. A., Rieke G. H., Lada E. A., Bouvier J., Lada C. J., 2003, ApJ, 593, 1093
Mac Low M.-M., Klessen R. S., 2004, Rev. Mod. Phys., 76, 125
Mamajek E. E., 2008, Astron. Nachr., 329, 10
McKee C. F., Ostriker E. C., 2007, ARA&A, 45, 565
McMillan S. L. W., Vesperini E., Portegies Zwart S. F., 2007, ApJ, 655, L45
Muench A. A., Lada C. J., Luhman K. L., Muzerolle J., Young E., 2007, AJ, 134, 411
Myers P. C., 2001, in Montmerle T., André P., eds, ASP Conf. Ser. Vol. 243, From Darkness to Light: Origin and Evolution of Young Stellar Clusters. Astron. Soc. Pac., San Francisco, p. 131
Myers P. C., Ho P. T. P., Schneps M. H., Chin G., Pankonin V., Winnberg A., 1978, ApJ, 220, 864
Myers P. C., Ladd E. F., Fuller G. A., 1991, ApJ, 372, L95
Padgett D. L. et al., 2008, ApJ, 672, 1013
Padoan P., Nordlund Å., 2005, in Corbelli E., Palla F., Zinnecker H., eds, Astrophys. Space Sci. Library Vol. 327, The Initial Mass Function 50 Years Later. Springer, Dordrecht, p. 357
Prim R. C., 1957, Bell Syst. Tech. J., 36, 1389
Rebull L. M. et al., 2007, ApJS, 171, 447
Ridge N. A., Schnee S. L., Goodman A. A., Foster J. B., 2006, ApJ, 643, 932
Schmeja S., Klessen R. S., 2004, A&A, 419, 405
Schmeja S., Klessen R. S., 2006, A&A, 449, 151
Schmeja S., Klessen R. S., Froebrich D., 2005, A&A, 437, 911
Straižys V., Černis K., Bartašiūtė S., 1996, Baltic Astron., 5, 125
Tafalla M., Myers P. C., Caselli P., Walmsley C. M., Comito C., 2002, ApJ, 569, 815
Tafalla M., Kumar M. S. N., Bachiller R., 2006, A&A, 456, 179
Teixeira P. S. et al., 2006, ApJ, 636, L45
von Hoerner S., 1963, Z. Astrophys., 57, 47
Wilking B. A., Meyer M. R., Greene T. P., Mikhail A., Carlson G., 2004, AJ, 127, 1131

This paper has been typeset from a TEX/LATEX file prepared by the author.